Nonadiabatic spectral redshift of high-order harmonics with the help of a VUV pulse

Hongchuan Du,[1,*] Shan Xue,[1] Huiqiao Wang,[2] Zhilei Zhang,[2] and Bitao Hu[1,†]
[1]*School of Nuclear Science and Technology, Lanzhou University, Lanzhou 730000, China*
[2]*Institute of Modern Physics, Chinese Academy of Sciences, Lanzhou 730000, China*
(Received 26 March 2015; published 30 June 2015)

We theoretically investigate the nonadiabatic spectral redshift of high-order harmonics with the help of a VUV pulse. It is found that the nonadiabatic spectral redshift of high-order harmonics can be observed when a weak VUV pulse is properly added in the falling part of the fundamental laser due to the nonadiabatic response of the dipole to rapid change of laser intensity. Further time-frequency analysis shows that the high-order harmonics are mainly generated in the falling part of the fundamental pulse. This is because the VUV pulse enhances the ionization in the falling part of the fundamental pulse by the *1s-2p* transition of He^+. In addition, this scheme is also used to observe the nonadiabatic spectral blueshift of high-order harmonics by changing the time delay between the fundamental laser and the VUV pulse.

DOI: 10.1103/PhysRevA.91.063844 PACS number(s): 42.65.Ky, 42.50.Hz, 32.80.Rm

I. INTRODUCTION

The high-order harmonic is one of the most fundamental phenomena occurring in the interaction of strong laser fields with atoms and molecules [1–6]. It provides us an important tool to generate coherent attosecond pulses, which can be used to investigate ultrafast electronic dynamics [7–9]. The physical mechanism of high-order harmonic generation (HHG) can be well described by a three-step model [10] In this model, an electron is first ionized by tunneling through the potential barrier when atoms and molecules are exposed to intense laser. Then it is accelerated by the laser field and acquires additional kinetic energy, and finally it can recombine with the parent ion. During the recombination process, a photon is emitted with the maximal energy given by $E_{\rm off} = I_p + 3.17U_p$, which successfully explains the cutoff of HHG observed in atoms [10].

With the development of ultrafast optics, intense few-cycle laser pulses have been produced routinely [11–13]. The electric-field amplitude of such a pulse will change significantly during one optical cycle, which enables the investigation of the nonadiabatic effects. In the rising part of the laser pulse, the effective amplitude of the successive laser cycle is larger than the previous one. Then the rising part of the laser field leads to a positive chirp in HHG, leading to a blueshift of single-atom high-order harmonics. In the falling part of the laser pulse, the effective amplitude of the successive laser cycle is smaller than the previous one. Then the falling part of the laser field leads to a negative chirp in HHG, leading to a redshift of single-atom high-order harmonics. For low-intensity laser pulses, no net spectral shift of high-order harmonics is observed due to the balance between the blueshift and the redshift. However, once this balance is broken, the nonadiabatic spectral blueshift or redshift of high-order harmonics would be observed. On the basis of this, Watson *et al.* predicted that the spectral blueshift of single-atom high-order harmonics can be observed when the ground state is completely depleted before the peak intensity is reached [14], which has been experimentally observed [15–17]. However, to our best knowledge, the nonadiabatic spectral redshift has not yet been reported in experiments. Recently, Bian and Bandrauk demonstrated that the nonadiabatic spectral redshift can be observed in the HHG of the polar diatomic molecule HeH^{2+} by means of the enhanced excitation of localized long lifetime excited states in the falling part of the laser pulse [18]. Unfortunately, the ground-state $1s\sigma$ of the HeH^{2+} is repulsive and unstable [19,20]. Moreover, the redshift decreases with the increasing orientation angle as shown in Ref. [21]. These limit the use of their scheme. Since a proper VUV pulse can efficiently assist the transition between ground state and excited states, Ishikawa *et al.* significantly enhanced the high-order harmonic emission from He^+ by the simultaneous irradiation of fundamental laser and high-order harmonic pulses [22,23]. This motivates the current work. In this work, we investigate the nonadiabatic spectral redshift of high-order harmonics by adding a weak VUV pulse in the falling part of the fundamental laser. In the study, the 13th-order harmonic pulse of the 400-nm fundamental laser is used to excite the electron from the *1s* state to the *2p* state since its photon energy is close to the *1s-2p* transition energy of He^+.

II. THEORETICAL METHODS

In order to probe the nonadiabatic effects, we numerically solve the three-dimensional (3D) time-dependent Schrodinger equation (TDSE) describing the interaction between the linearly polarized laser field and the He^+ ion. The TDSE for the full wave function can be expressed as

$$i\frac{\partial}{\partial t}\psi(\mathbf{r},t) = \left[-\frac{\nabla^2}{2} - \frac{2}{r} + W(\mathbf{r},t)\right]\psi(\mathbf{r},t), \qquad (1)$$

where atomic units are used throughout unless otherwise stated. The laser-matter interaction term is defined as

$$W(\mathbf{r},t) = \begin{cases} -\mathbf{r}\cdot\mathbf{E}(t) & \text{(length gauge)} \\ i\mathbf{A}(t)\cdot\nabla & \text{(velocity gauge)} \end{cases}. \qquad (2)$$

Here $\mathbf{E}(t) = -\partial_t\mathbf{A}(t)$ is the electric field and $\mathbf{A}(t)$ is the corresponding vector potential of the laser pulse. The time-dependent wave function can be obtained by numerically solving Eq. (1) in the spherical coordinate system using the

*duhch@lzu.edu.cn
†hubt@lzu.edu.cn

Crank-Nicolson method [24,25]. Then the dipole acceleration can be obtained by employing Ehrenfest's theorem:

$$a(t) = -\langle\psi(\mathbf{r},t)|\frac{\cos\theta}{r^2} - E(t)|\psi(\mathbf{r},t)\rangle. \quad (3)$$

Then the HHG spectrum is given by

$$P_A(\omega) = \left|\frac{1}{\sqrt{2\pi}}\int_{-\infty}^{+\infty} a(t)\exp(-i\omega t)dt\right|^2, \quad (4)$$

where ω is the frequency of the high-order harmonics.

III. RESULTS AND DISCUSSIONS

In order to illustrate our scheme, we first present the electric fields in Fig. 1. In our scheme, a 400-nm laser pulse is adopted as the driving pulse, and its 13th harmonic pulse is used to enhance the efficiency of HHG in the falling part of the fundamental pulse since it can excite the electron from the *1s* state to the *2p* state of He^+. As a result, the balance between the blueshift and the redshift is broken, which leads to the redshift of high-order harmonics. The vector potential of the combined field is expressed as

$$A(t) = A_0\cos^2\left(\frac{\pi t}{\tau_0}\right)\sin(\omega_0 t) + A_1\exp\left[-2\ln(2)(t+t_{\text{delay}})^2/\tau_1^2\right]\cos(\omega_1 t). \quad (5)$$

Here, ω_0 and ω_1 are the frequencies of the fundamental pulse and its 13th harmonic pulse, respectively. A_0 and A_1 are the vector-potential amplitudes of the two pulses, respectively. τ_0 and τ_1 are the total duration of the fundamental pulse and the full width at half maximum of the 13th harmonic pulse, respectively. t_{delay} is the time delay between the two pulses. Then the electric field can be given by $E(t) = -\partial_t A(t)$. Thus the total electric-field area is zero. In the calculation, we set $A_0 = E_0/\omega_0$ and $A_1 = E_1/\omega_1$, where E_0 and E_1 are equal to 0.307 and 0.0614 a.u. τ_0 and τ_1 are chosen to be $15T_0$ and $3T_0$, where T_0 is the optical period of the fundamental pulse. t_{delay} is equal to $-2T_0$.

In order to demonstrate this scheme, Fig. 2 presents the harmonic spectrum in the velocity gauge by exposing He^+ to the combined field. As shown in this figure, this harmonic spectrum shows the general characteristics of the usual HHG spectra except the strong resonance around the 13th-order harmonic. The harmonic intensity in this region is about six orders higher than that of the harmonics in the plateau. This is because we adopt the 13th-order harmonic pulse of the fundamental pulse in the calculation. Another important feature of the spectrum is the spectral redshift, which is shown in the inset of Fig. 2. For the sake of checking the accuracy and stability of our results, we compare the calculated HHG spectra in the velocity gauge and the length gauge in Fig. 3. As shown in this figure, there is a good agreement between the two gauges, which implies that the spectral redshift of the harmonics does not come from the calculation error. Although the two gauges give the same physical results, a much smaller maximum value of L is needed for a converged result in the velocity gauge than that needed in the length gauge. Therefore, the velocity gauge is used in the next section. For comparison,

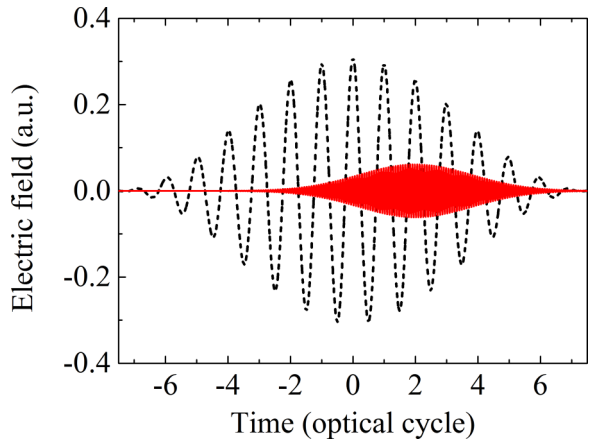

FIG. 1. (Color online) Electric fields of the 400-nm driving pulse (dashed black curve) and the VUV pulse (solid red curve).

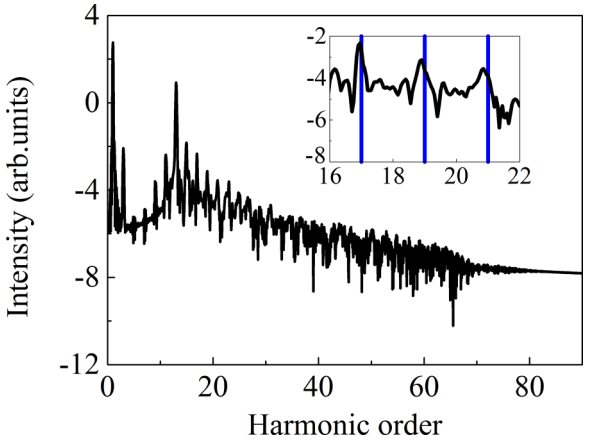

FIG. 2. (Color online) The harmonic spectrum produced by exposing He^+ to the combined field. Inset: Spectral structure of some harmonics illustrating the presence of redshifted harmonics.

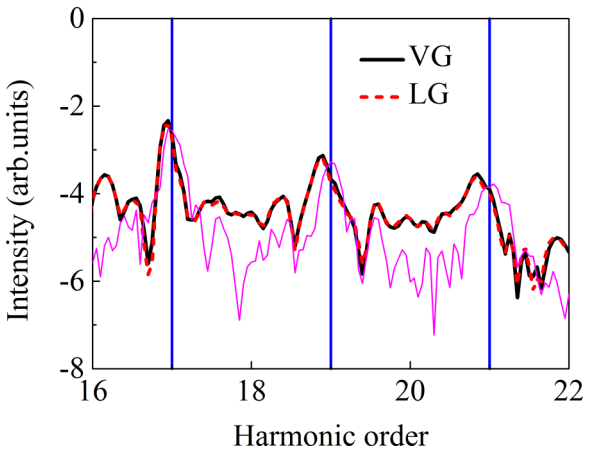

FIG. 3. (Color online) Spectral structure of some harmonics produced by exposing He^+ to the combined field. The thick curves and thin curve are the results at $t_{\text{delay}} = -2T_0$ and 0, respectively. VG, velocity gauge; LG, length gauge. Other parameters are the same as in Fig. 2.

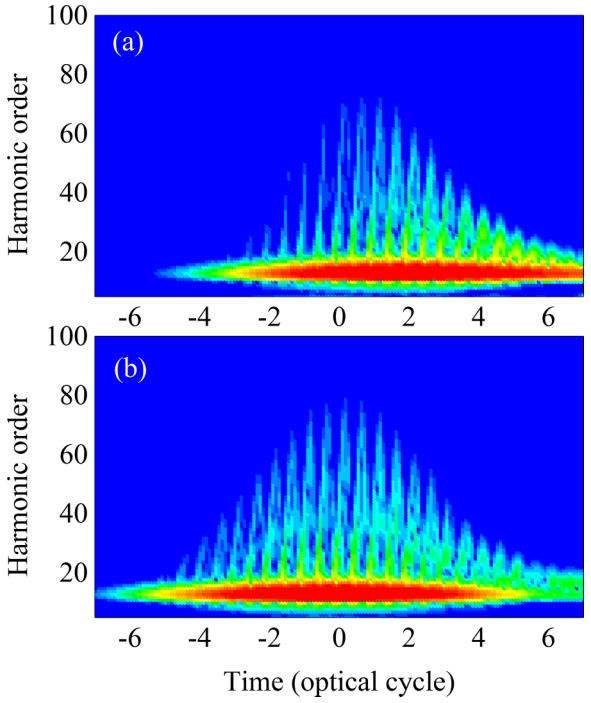

FIG. 4. (Color online) Time-frequency distribution of the harmonic spectra generated with (a) $t_{\text{delay}} = -2T_0$ and (b) $t_{\text{delay}} = 0$. The same color scale is used in the two pictures.

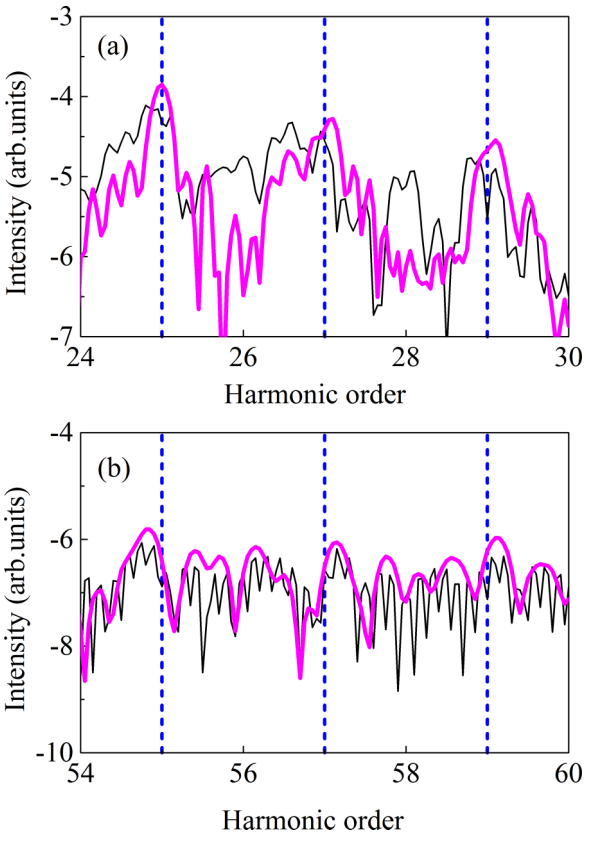

FIG. 5. (Color online) Spectral structure of the (a) 24th–30th harmonics and (b) 54th–60th harmonics. $t_{\text{delay}} = -2T_0$ (thin solid black curve) and $t_{\text{delay}} = 0$ (thick solid pink curve).

Fig. 3 also shows the HHG spectrum calculated with $t_{\text{delay}} = 0$ (thin solid pink curve). It is clear that no spectral redshift of the harmonics is observed in this case. This is because the efficiency of HHG in the rising part is equal to that in the falling part of the fundamental pulse when the 13th harmonic pulse is superimposed to the fundamental pulse with $t_{\text{delay}} = 0$.

To further confirm the above conclusions, we perform a time profile analysis of the harmonic spectrum in Fig. 2 to probe the temporal structures. The results are shown in Fig. 4(a). For comparison, Fig. 4(b) presents the time-frequency distribution of the harmonic spectrum generated with $t_{\text{delay}} = 0$. From the figures, one can see an obvious resonance area around the 13th-order harmonic for the two cases, which comes from the electron transition from the *2p* state to the *1s* state. In addition, there is also an obvious difference between the two cases. For the case of $t_{\text{delay}} = 0$, as shown in Fig. 4(b), the efficiency of HHG is symmetrical about $t = 0$. Namely, the efficiency of HHG in the rising part is comparative with that in the falling part of the fundamental pulse. Thus no net shift of high-order harmonics is observed due to the balance between the blueshift and the redshift. However, for the case of $t_{\text{delay}} = -2T_0$, it can be seen from Fig. 4(a) that the efficiency of HHG is larger in the falling part than that in the rising part of the fundamental pulse. Hence, the redshift is dominated, and the nonadiabatic spectral redshift can be observed as shown in Fig. 2. These are in good agreement with the above conclusions. In addition, it is also noted that the resonance area around the 13th harmonic has a considerable energy width, which covers the harmonic range chosen to demonstrate the shift effect. Therefore, there is the following question: can the obvious spectral redshift be observed outside the chosen region? In order to answer this question, we present the spectral structure of the 24th–30th harmonics and 54th–60th harmonics in Fig. 5, respectively. For comparison, we also show the spectral structure of the corresponding harmonics calculated with $t_{\text{delay}} = 0$. For the 24th–30th harmonics in the plateau, as shown in Fig. 5(a), the obvious spectral redshift can be still seen. However, for the 54th–60th harmonics in the cutoff, as shown in Fig. 5(b), there are no clear peaks of high-order harmonics. Therefore, we have to choose the harmonics generated at $t_{\text{delay}} = 0$ as a benchmark to judge whether or not the spectral redshift takes place. One can see that there is no obvious spectral redshift of the harmonics in the cutoff, which is in accordance with the results in Ref. [18]. This is because the harmonics near the cutoff mainly occur only around the peak laser intensity, where the change of laser intensity is small near the peak.

Next, we further investigate the influence of the laser parameters. Figure 6 shows the spectral structures of some harmonics produced at different intensities of the VUV pulse. In the calculation, we choose four different intensities of the VUV pulse. They are $E_1 = 0.0614$ a.u. (thick solid pink curve), $E_1 = 0.0307$ a.u. (thick dashed blue curve), $E_1 = 0.01535$ a.u. (thick dotted red curve), and $E_1 = 0.00307$ a.u. (thin dashed black curve), respectively. It can be clearly seen that the spectral redshift of these harmonics hardly changes for the large intensity-region of the VUV pulse. This implies that this scheme is stable against the intensity shift of the VUV pulse. Besides, we also investigate the intensity influence of the fundamental pulse to the spectral redshift, which is

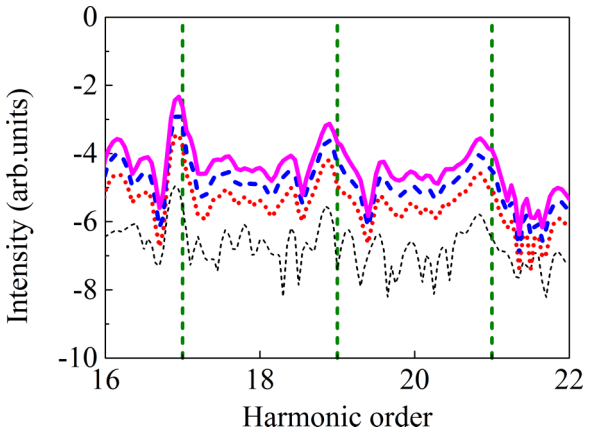

FIG. 6. (Color online) Spectral structure of some harmonics produced at different intensities of the VUV pulse. Other parameters are the same as in Fig. 2.

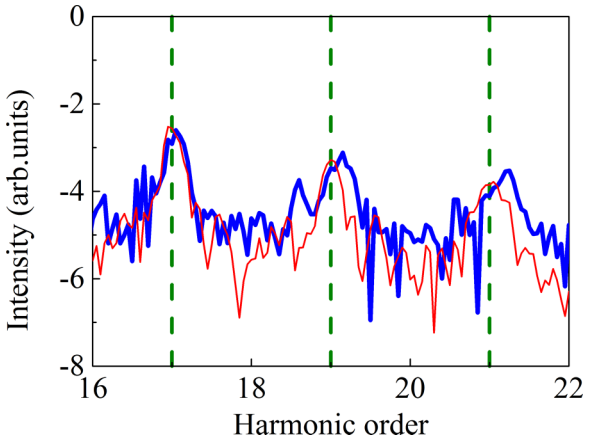

FIG. 8. (Color online) Spectral structure of some harmonics produced at $t_{\text{delay}} = 2T_0$. Other parameters are the same as in Fig. 2.

shown in Fig. 7. In the calculation, we choose three different intensities. They are $E_0 = 0.307$ a.u. (thin solid black curve), $E_0 = 0.239$ a.u. (thin dotted red curve), and $E_0 = 0.169$ a.u. (thick solid blue curve). It is found that the spectral redshift decreases as the intensity of the fundamental pulse decreases. This can be understood by the three-step model [10]. In this model, the electron is ejected and then recollides, producing harmonics. If the peak field amplitude decreases during the laser cycle, then the recolliding electron will experience a phase shift relative to the field. This leads to the spectral redshift of harmonics. Hence, the redshift is proportional to the rate of field decrease, which is similar to the results about blueshift in Ref. [14]. Therefore, the change of the intensity dI/dt must be large enough to observe the obvious redshift. There are two ways of increasing dI/dt. First, we can adopt the laser pulses with shorter duration. However, this way will reduce the number of the quantum trajectories, and finally lead to no clear peaks of high-order harmonics in the spectra. In this case, it will be very difficult to observe the redshift. Second, we can adopt the laser pulses with more intense intensity. In this case, if the target atom with small ionization energy is chosen,

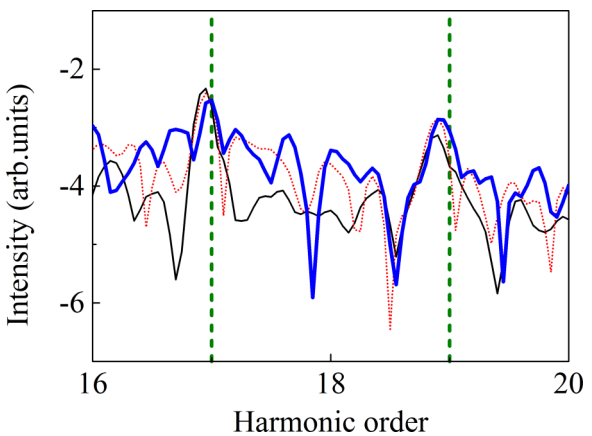

FIG. 7. (Color online) Spectral structure of some harmonics produced at different intensities of the fundamental pulse. Other parameters are the same as in Fig. 2.

the ionization of the target atom in the rising of the laser pulse would be comparative with that in the falling part. Then we cannot observe the obvious redshift. This is the reason why we choose the He^+ as the target atom in the calculation.

In order to demonstrate that this scheme is high-powered, we also study the spectral blueshift of high-order harmonics by changing the time delay between the fundamental laser and the VUV pulse. These results are presented in Fig. 8. For comparison, the spectrum generated at $t_{\text{delay}} = 0$ is also presented. As shown in this figure, the spectral blueshift can be observed by setting $t_{\text{delay}} = 2T_0$. This implies that this scheme can be also used to observe the nonadiabatic spectral blueshift of high-order harmonics by properly choosing the time delay between the fundamental laser and the VUV pulse. It is worth noting that our mechanism is entirely different from that of Refs. [15–17] though the spectral blueshift is also observed in their works. In Refs. [15–17], the spectral blueshift comes from the fact that the ground state is completely depleted before the peak intensity is reached, which leads to the quench of HHG in the falling part of the laser pulse. However, in our case, the ionization probability is about 0.26 at the end of the laser pulse according to our calculation. The spectral blueshift occurs because we break the ionization balance between the rising part and the falling part of the laser pulse by placing the harmonic pulse in the rising part of the IR pulse.

Finally, we discuss the experimental access to observe the nonadiabatic spectral redshift. In the HHG process, the intense laser interacts with a lot of atoms (ions) and creates free electrons, which induces a change of refractive index. The variation of the refractive index leads to a blueshift of the fundamental laser field. The shift can be estimated by the following expression (in SI units) [26]:

$$\triangle\lambda = -\frac{e^2\lambda_0^3}{8\pi^2\epsilon_0 m_e c^3}\frac{dN_e}{dt}L, \tag{6}$$

where L is the propagation length, and N_e is the electron density. For HHG with order n, the blueshift mainly comes from the shift $\triangle\lambda_1$ induced by the shift of the fundamental field. $\triangle\lambda_1$ is proportional to $\triangle\lambda/n$. We should adopt a thin gas target with a low density to reduce this influence of propagation effects. Next, we assume that the gas target has a density of

7×10^{17} atoms/cm^3 (20 Torr), and the propagation length L is equal to 0.5 mm. For the case in Fig. 2, the ionization probability is about 0.25 according to our calculation. Then the calculated blueshift of the fundamental laser field is 0.417 nm by Eq. (6). For the 21st-order harmonic, the blueshift is about 0.02 nm. However, the expected nonadiabatic spectral redshift is about 0.156 nm. Therefore, we predict that the nonadiabatic spectral redshift can be observed by means of this scheme in the near future.

IV. CONCLUSION

In summary, we theoretically investigate the nonadiabatic spectral redshift of high-order harmonics with the help of a VUV pulse. It is found that the nonadiabatic spectral redshift of high-order harmonics can be observed when a weak VUV pulse is properly added in the falling part of the fundamental laser. Moreover, this scheme is stable against the intensity shift of the VUV pulse. We also found that the intensity of the fundamental pulse is not too small in order to observe obvious spectral redshift. In addition, this method is also suitable to observe the nonadiabatic spectral blueshift of high-order harmonics by properly choosing the time delay between the fundamental laser and the VUV pulse. We predict that the nonadiabatic spectral redshift can be observed by means of this scheme in the near future by comparing the nonadiabatic spectral redshift with the blueshift induced by propagation effects.

ACKNOWLEDGMENTS

The information of funding providers is correct. This work was supported by the National Natural Science Foundation of China (Grants Nos. 11404153, No. 11135002, No. 11175076, No. 11475076, and No. 11405077) and the Fundamental Research Funds for the Central Universities of China (Grants Nos. lzujbky-2014-10, No. lzujbky-2014-13, and No. lzujbky-2014-14).

[1] A. McPherson, G. Gibson, H. Jara, U. Johann, T. S. Luk, I. A. McIntyre, K. Boyer, and C. K. Rhodes, J. Opt. Soc. Am. B **4**, 595 (1987).
[2] T. Brabec and F. Krausz, Rev. Mod. Phys. **72**, 545 (2000).
[3] A. Rundquist, C. G. Durfee III, Z. H. Chang, C. Herne, S. Backus, M. M. Murnane, and H. C. Kapteyn, Science **280**, 1412 (1998).
[4] E. J. Takahashi, T. Kanai, K. L. Ishikawa, Y. Nabekawa, and K. Midorikawa, Phys. Rev. Lett. **101**, 253901 (2008).
[5] J. Itatani, D. Zeidler, J. Levesque, M. Spanner, D. M. Villeneuve, and P. B. Corkum, Phys. Rev. Lett. **94**, 123902 (2005).
[6] R. de Nalda, E. Heesel, M. Lein, N. Hay, R. Velotta, E. Springate, M. Castillejo, and J. P. Marangos, Phys. Rev. A **69**, 031804(R) (2004).
[7] F. Krausz and M. Ivanov, Rev. Mod. Phys. **81**, 163 (2009).
[8] R. Kienberger, E. Goulielmakis, M. Uiberacker, A. Baltuska, V. Yakovlev, F. Bammer, A. Scrinzi, Th. Westerwalbesloh, U. Kleineberg, U. Heinzmann, M. Drescher, and F. Krausz, Nature (London) **427**, 817 (2004).
[9] M. I. Stockman, M. F. Kling, U. Kleineberg, and F. Krausz, Nat. Photonics **1**, 539 (2007).
[10] P. B. Corkum, Phys. Rev. Lett. **71**, 1994 (1993).
[11] E. Goulielmakis, M. Schultze, M. Hofstetter, V. S. Yakovlev, J. Gagnon, M. Uiberacker, A. L. Aquila, E. M. Gullikson, D. T. Attwood, R. Kienberger, F. Krausz, and U. Kleineberg, Science **320**, 1614 (2008).
[12] L. Gallmann, D. H. Sutter, N. Matuschek, G. Steinmeyer, U. Keller, C. Iaconis, and I. A. Walmsley, Opt. Lett. **24**, 1314 (1999).
[13] L. Xu, G. Tempea, Ch. Spielmann, F. Krausz, A. Stingl, K. Ferencz, and S. Takano, Opt. Lett. **23**, 789 (1998).
[14] J. B. Watson, A. Sanpera, and K. Burnett, Phys. Rev. A **51**, 1458 (1995).
[15] H. J. Shin, D. G. Lee, Y. H. Cha, K. H. Hong, and C. H. Nam, Phys. Rev. Lett. **83**, 2544 (1999).
[16] C.-G. Wahlström, J. Larsson, A. Persson, T. Starczewski, S. Svanberg, P. Salières, Ph. Balcou, and A. L'Huillier, Phys. Rev. A **48**, 4709 (1993).
[17] K. Miyazaki and H. Takada, Phys. Rev. A **52**, 3007 (1995).
[18] X.-B. Bian and A. D. Bandrauk, Phys. Rev. A **83**, 041403 (2011).
[19] G. Lagmago Kamta and A. D. Bandrauk, Phys. Rev. A **76**, 053409 (2007).
[20] I. Ben-Itzhak, I. Gertner, O. Heber, and B. Rosner, Phys. Rev. Lett. **71**, 1347 (1993).
[21] X.-B. Bian and A. D. Bandrauk, Appl. Sci. **3**, 267 (2013).
[22] K. Ishikawa and K. Midorikawa, Phys. Rev. A **65**, 043405 (2002).
[23] K. Ishikawa, Phys. Rev. Lett. **91**, 043002 (2003).
[24] J. Crank and P. Nicolson, Proc. Cambridge Philos. Soc. **43**, 50 (1947).
[25] G. D. Smith, *Numerical Solution of Partial Differential Equations*, 3rd ed. (Clarendon, Oxford, 1985).
[26] S. C. Rae and K. Burnett, Phys. Rev. A **46**, 1084 (1992).